A Path Integral Time-Domain Method for Electromagnetic Scattering

Robert D. Nevels, Jeffrey A. Miller, and Richard E. Miller

***Abstract*—A new full wave time-domain formulation for the electromagnetic field is obtained by means of a path integral. The path integral propagator is derived via a state variable approach starting with Maxwell's differential equations in tensor form. A numerical method for evaluating the path integral is presented and numerical dispersion and stability conditions are derived and numerical error is discussed. An absorbing boundary condition is demonstrated for the one-dimensional (1-D) case. It is shown that this time domain method is characterized by the unconditional stability of the path integral equations and by its ability to propagate an electromagnetic wave at the Nyquist limit, two numerical points per wavelength. As a consequence the calculated fields are not subject to numerical dispersion. Other advantages in comparison to presently popular time-domain techniques are that it avoids time interval interleaving and it does not require the methods of linear algebra such as basis function selection or matrix methods.**

***Index Terms*—Electromagnetic scattering, path-integral methods, transient scattering.**

I. Introduction

ORIGINALLY developed as an alternative to the Schrodinger and Heisenberg treatments of quantum mechanics [1], the Feynman path integral is neither an integral nor differential equation. It is most appropriately described as a propagator equation, which is an expression that propagates a source function through successive time steps. However, there are only a few exact analytical solutions for the electromagnetic field via a path integral formulation [2]. Often even relatively simple problem geometries, such as a source over a conducting half-space, require a foreknowledge of the result [3]. This was the case even, for example, in early research centered on the calculation of the classical wedge diffraction coefficients, which were obtained previously using Keller's geometrical theory of diffraction [4]. Following the work by Keller and McLaughlin [5] and Bushlaev [6], who was the first to suggest using the path integral to derive diffraction coefficients for the perfectly conducting wedge, there have been a number of variations and improvements on the original wedge diffraction solution scheme. However, there are examples in electromagnetics where statistical or asymptotic methods have been used to solve the path integral, yielding an original analytical or a numerical result.

Manuscript received May 26, 1998; revised November 29, 1999. This work was supported by the National Science Foundation under Grants ECS-9811094 and ECS 9820644.

The authors are with the Department of Electrical Engineering, Texas A&M University, College Station, TX 77843-3128 USA.

Publisher Item Identifier S 0018-926X(00)03250-6.

Klyatskin and Tatarskii [7] first suggested employing the path integral to investigate wave propagation in random media. It soon became widely used in similar applications such as for example the work by Chow [8] on laser beam propagation. By means of asymptotic methods for the evaluation of path integrals, Dashen [9] obtained expressions for arbitrary moments of wave intensity in the regime of saturated fluctuations. Zavarotny [10] derived corrections to the intensity moments and Besieris [11] has analyzed $2N$th-order multifrequency coherence functions. Recently, there has been considerable interest in what is known as the two-scale path integral expansion for wave propagation in random media, which, as shown by Gozani [12], is not an asymptotic method as was previously thought.

Several studies have been carried out in which path integral methods are used to investigate electromagnetic wave propagation in the atmosphere and in optical waveguides. Eve [13] used analytical methods to obtain the path integral propagator in a stratified dielectric wave guiding system. More recently, Constantinou and Jones [14] have derived the path integral propagator for a linearly tapering graded index waveguide. A class of numerical path integral propagation methods, often described as parabolic wave equation methods, has become increasingly popular primarily due to the Fourier split-step algorithm introduced by Hardin and Tappet [15]. There have been several improvements in this method, including hybrid solutions such as what can be described as the path-integral/radio-physical optics hybrid model for tropospheric propagation recently reported by Hitney [16]. For lower atmosphere propagation, Dockery and Kuttler [17] developed an improved impedance-boundary algorithm.

Most of the electromagnetics research described above has been carried out in the frequency domain, relying upon Helmholtz equation, an elliptic equation, as the starting point. However, in order to apply path integral methods, Helmholtz equation must be converted to a parabolic or hyperbolic equation. A parabolic equation can be obtained by either making use of what is known as a parabolic approximation, or by operator-splitting techniques. Both of these methods allow only small changes as a function of distance in the refractive index profile in one direction. Although this is sufficient for wave propagation studies, these approximations effectively prohibit electromagnetic scattering analysis for all but elementary objects or boundaries. Nevels *et al.* [18] were able to avoid restrictions on the index of diffraction by a transformation technique, but this approach is constrained to scalar scattering applications and it is computationally time consuming.

The path integral time-domain method (PITD) introduced here is, to the authors' knowledge, the first successful full wave

electromagnetic field scattering formulation based on the path integral and also the first complete path integral expression for electromagnetic field scattering in the time domain. It has several attractive features. At each successive time step the time-domain propagator yields the six electric and magnetic field intensity components throughout the scattering region. Boundary and radiation conditions are manifest in its expression and therefore do not have to be imposed during numerical evaluation. A primary advantage is that it is not difficult to develop a PITD computer code, as compared to other time domain methods, because the path integral expression in phase space can be evaluated by the standard fast Fourier transform.

Below, the full wave path integral time-domain equations are derived. A method for numerically evaluating of the PITD equations is presented and its associated numerical dispersion and stability conditions are derived. The numerical error of the proposed method is discussed and an absorbing boundary condition in one-dimension is implemented. Results are presented that demonstrate its effectiveness in terms of accuracy, stability, numerical speed, and field absorption at the numerical boundary. In the analysis below the time convention is $\exp(j\omega t)$.

II. Analysis

In a source-free inhomogeneous region the time-domain Maxwell curl equations in terms of the electric and magnetic field intensities $\mathbf{E}$ and $\mathbf{H}$ are

$$\nabla \times \mathbf{E} = -\mathbf{J}_m - \mu \frac{\partial \mathbf{H}}{\partial t} \tag{1}$$

$$\nabla \times \mathbf{H} = \mathbf{J}_e + \varepsilon \frac{\partial \mathbf{E}}{\partial t} \tag{2}$$

where μ and ε are the permeability and permittivity for an inhomogeneous region. The medium electric conductivity σ is related to the electric field through the electric conduction current $\mathbf{J}_e$ by

$$\mathbf{J}_e = \sigma \mathbf{E} \tag{3}$$

and similarly the medium magnetic resistivity ρ^* is related to the magnetic field through the magnetic conduction current $\mathbf{J}_m$ by

$$\mathbf{J}_m = \rho^* \mathbf{H}. \tag{4}$$

Equations (3) and (4) are substituted into (1) and (2), which can be rearranged to give

$$\frac{\partial \mathbf{E}}{\partial t} = -\frac{\sigma \mathbf{E}}{\varepsilon} + \frac{1}{\varepsilon} \nabla \times \mathbf{H} \tag{5}$$

$$\frac{\partial \mathbf{H}}{\partial t} = -\frac{1}{\mu} \nabla \times \mathbf{E} - \frac{\rho^* \mathbf{H}}{\mu}. \tag{6}$$

Equations (5) and (6) can be cast in the general matrix form

$$\frac{\partial \mathbf{F}}{\partial t} = \bar{\mathbf{S}} \mathbf{F} \tag{7}$$

with the field vector $\mathbf{F}$ defined by

$$\mathbf{F} = [\, E_x \quad E_y \quad E_z \quad H_x \quad H_y \quad H_z \,]^T \tag{8}$$

and the 6×6 matrix operator expressed symbolically by

$$\bar{\mathbf{S}} = \begin{bmatrix} -\frac{\sigma}{\varepsilon} & \frac{1}{\varepsilon} \nabla \times \\ -\frac{1}{\mu} \nabla \times & -\frac{\rho^*}{\mu} \end{bmatrix}. \tag{9}$$

The solution to (7), which is a vector hyperbolic equation, can be placed in path integral form by first finding a propagator [19] matrix $\bar{\mathbf{K}}(\mathbf{r}, \mathbf{r}'; t, t')$ that satisfies

$$\frac{\partial \bar{\mathbf{K}}}{\partial t} = \overline{\mathbf{SK}} \tag{10}$$

subject to the initial condition

$$\lim_{t \to t'} \bar{\mathbf{K}} = \bar{\mathbf{I}} \delta(\mathbf{r} - \mathbf{r}'). \tag{11}$$

Here $\bar{\mathbf{I}}$ is the identity matrix, t' and t, respectively, are the initial and current times, $\delta(\mathbf{r} - \mathbf{r}')$ is the Dirac delta function and $\mathbf{r}'$ and $\mathbf{r}$ are the initial and current spatial positions with $\mathbf{r} = x\hat{\mathbf{x}} + y\hat{\mathbf{y}} + z\hat{\mathbf{z}}$. By substitution it can be shown that a solution to (10) is

$$\bar{\mathbf{K}} = e^{\bar{\mathbf{S}} t} \bar{\mathbf{K}}_o. \tag{12}$$

The coefficient $\bar{\mathbf{K}}_o$ can be found by enforcing (11), which gives

$$\bar{\mathbf{K}} = e^{\bar{\mathbf{S}}(t - t')} \delta(\mathbf{r} - \mathbf{r}'). \tag{13}$$

An inverse Fourier transform representation

$$\delta(\mathbf{r} - \mathbf{r}') = \frac{1}{(2\pi)^3} \int_{-\infty}^{\infty} e^{j\mathbf{k} \cdot (\mathbf{r} - \mathbf{r}')} \, d\mathbf{k} \tag{14}$$

of the delta function in (13) gives the complete propagator expression

$$\bar{\mathbf{K}} = \frac{1}{(2\pi)^3} \int_{-\infty}^{\infty} e^{\bar{\mathbf{S}} \tau} e^{j\mathbf{k} \cdot (\mathbf{r} - \mathbf{r}')} \, d\mathbf{k}. \tag{15}$$

Here $\tau = t - t'$ is the time increment between the initial and current times. The differential $d\mathbf{k} = dk_x dk_y dk_z$ and $\mathbf{k} = k_x \hat{\mathbf{x}} + k_y \hat{\mathbf{y}} + k_z \hat{\mathbf{z}}$ are in terms of the spatial frequency components k_x, k_y and k_z. The matrix exponential $e^{\bar{\mathbf{S}} \tau}$ is then expanded in the power series

$$e^{\bar{\mathbf{S}} \tau} = \bar{\mathbf{I}} + \bar{\mathbf{S}} \tau + \bar{\mathbf{S}}^2 \tau^2 / 2 + \bar{\mathbf{S}}^3 \tau^3 / 3 + \cdots \tag{16}$$

each term of which is allowed to operate on the Fourier basis function $e^{j\mathbf{k} \cdot \mathbf{r}}$. This operation creates a new matrix $\bar{\mathbf{S}}(\mathbf{r}, \mathbf{k})$ in which the differential operators are replaced according to $\partial / \partial x \to jk_x$, $\partial / \partial y \to jk_y$, and $\partial / \partial z \to jk_z$. The series is resumed producing a matrix exponential $e^{\bar{\mathbf{S}}(\mathbf{r}, \mathbf{k}) \tau}$.

Next any one of a number of methods can be used to reduce the matrix exponential $e^{\bar{\mathbf{S}}(\mathbf{r}, \mathbf{k}) \tau}$ to a standard 6×6 matrix $\bar{\mathbf{A}}(\mathbf{r}, \mathbf{k})$. These include the eigenvalue, Cayley–Hamilton and resolvent matrix methods. The details of these methods can be found in the literature on state variables [20]. Our preference is the eigenvalue method because it can easily be used in conjunction with common PC math software.

The eigenvalue method consists of first finding the eigenvalues and the corresponding eigenvectors of $\bar{\mathbf{S}}(\mathbf{r},\mathbf{k})$. The eigenvectors comprise the modal matrix $\bar{\mathbf{M}}$ and the eigenvalues λ_i are incorporated in $e^{\lambda_i \tau}$ which form the diagonal matrix $\bar{\mathbf{P}}(\lambda)$. The matrix $\bar{\mathbf{A}}$ can then be found by taking the matrix product

$$\bar{\mathbf{A}} = \bar{\mathbf{M}}\bar{\mathbf{P}}(\lambda)\bar{\mathbf{M}}^{-1}. \tag{17}$$

For the special case of a loss free $(\sigma, \rho^* \to 0)$ inhomogeneous medium, the eigenvalue method yields the $\bar{\mathbf{A}}$ matrix components

$$\begin{aligned}
&A_{11} = A_{44} = \left\lfloor k_x^2 + \left(k_y^2 + k_z^2\right)\cos(k_o v\tau)\right\rfloor / k_o^2 \\
&A_{12} = A_{21} = A_{45} = A_{54} = k_x k_y[1 - \cos(k_o v\tau)]/k_o^2 \\
&A_{13} = A_{31} = A_{46} = A_{64} = k_x k_z[1 - \cos(k_o v\tau)]/k_o^2 \\
&A_{14} = A_{25} = A_{36} = A_{41} = A_{52} = A_{63} = 0 \\
&A_{15} = -A_{24} = -jk_z\eta\sin(k_o v\tau)/k_o \\
&A_{16} = -A_{34} = jk_y\eta\sin(k_o v\tau)/k_o \\
&A_{22} = A_{55} = \left[k_y^2 + \left(k_x^2 + k_z^2\right)\cos(k_o v\tau)\right]/k_o^2 \\
&A_{23} = A_{32} = A_{56} = A_{65} = k_y k_z[1 - \cos(k_o v\tau)]/k_o^2 \\
&A_{26} = -A_{35} = -jk_x\eta\sin(k_o v\tau)/k_o \\
&A_{33} = A_{66} = \left[k_z^2 + \left(k_x^2 + k_y^2\right)\cos(k_o v\tau)\right]/k_o^2 \\
&A_{42} = -A_{51} = jk_z\sin(k_o v\tau)/(k_o\eta) \\
&A_{43} = -A_{61} = -jk_y\sin(k_o v\tau)/(k_o\eta) \\
&A_{53} = -A_{62} = jk_x\sin(k_o v\tau)/(k_o\eta)
\end{aligned} \tag{18}$$

where $k_o^2 = k_x^2 + k_y^2 + k_z^2$ and $v = 1/\sqrt{\mu\varepsilon}$ and $\eta = \sqrt{\mu/\varepsilon}$ are the phase velocity and intrinsic impedance, which are functions of position in an inhomogeneous medium.

A field vector $\mathbf{F}_o$ can now be propagated one time increment τ by evaluating [19]

$$\mathbf{F}(\mathbf{r},t) = \int_{-\infty}^{\infty} \bar{\mathbf{K}}(\mathbf{r},\mathbf{r}';\tau)\mathbf{F}_o(\mathbf{r}',t')\,d\mathbf{r}' \tag{19}$$

(see Appendix) where $d\mathbf{r}' = dx'\,dy'\,dz'$. Substituting (15), with $e^{\bar{\mathbf{S}}\tau}$ replaced by $\bar{\mathbf{A}}$ above, into (19) gives

$$\mathbf{F}(\mathbf{r},t) = \frac{1}{(2\pi)^3}\int_{-\infty}^{\infty} \bar{\mathbf{A}}(\mathbf{r},\mathbf{k}) \times \left[\int_{-\infty}^{\infty} \mathbf{F}_o(\mathbf{r}',t')e^{-j\mathbf{k}\cdot\mathbf{r}'}d\mathbf{r}'\right] e^{j\mathbf{k}\cdot\mathbf{r}}d\mathbf{k}. \tag{20}$$

Equation (20) reveals that propagation of the field in time in an inhomogeneous region is accomplished by a spatial Fourier transformation of the initial field distribution followed by multiplication by the operator $\bar{\mathbf{A}}$ and subsequent spatial frequency domain inverse Fourier transformation. Because it is the operation that actually moves the wave, $\bar{\mathbf{A}}$ is referred to as the evolution operator or the transition matrix [1]. Equation (20) is all that is needed to propagate the field through a single-time increment τ. The resulting time stepped field $\mathbf{F}$ then becomes the new initial field $\mathbf{F}_o$ ready to be propagated another time increment. The complete expression for a field that has evolved through N successive time iterations starting at $t' = t_o$ and ending at time t is known as the path integral. The path integral for time evolution of the electromagnetic field, found by successive applications of (20), is therefore

$$\mathbf{F}(\mathbf{r},t) = \lim_{\tau \to 0} \frac{1}{(2\pi)^{3N}} \prod_{i=1}^{N} \int_{-\infty}^{\infty} \bar{\mathbf{A}}_i e^{j\mathbf{k}_i\cdot\mathbf{r}_i}\,d\mathbf{k}_i \times \int_{-\infty}^{\infty} \mathbf{F}_o(\mathbf{r}_o,t_o)e^{-j\mathbf{k}_i\cdot\mathbf{r}_{i-1}}d\mathbf{r}_{i-1}. \tag{21}$$

This equation can be expressed as a sequence of forward (F) and inverse (F^{-1}) Fourier transforms, written symbolically as

$$\mathbf{F}(\mathbf{r},t) = \lim_{\tau \to 0} \mathsf{F}^{-1}\{\bar{\mathbf{A}}_N \mathsf{F}\{\mathsf{F}^{-1}\{\bar{\mathbf{A}}_{N-1} \cdots \mathsf{F}\{\mathsf{F}^{-1}\{\bar{\mathbf{A}}_1 \mathsf{F}\{\mathbf{F}_o(\mathbf{r}_o,t_o)\}\}\}\cdots\}\}\}. \tag{22}$$

A. Analytical Example

As an example, consider the case of a 1-D plane wave with components E_z and H_y propagating in the x-direction in a homogeneous region. Equation (22) at the first time step is

$$\begin{bmatrix} E_z \\ H_y \end{bmatrix} = \frac{1}{2\pi}\int_{k_x} \begin{bmatrix} \cos(k_x v\tau) & j\eta\sin(k_x v\tau) \\ \frac{j}{\eta}\sin(k_x v\tau) & \cos(k_x v\tau) \end{bmatrix} \times \begin{bmatrix} \mathsf{F}\{E_z\} \\ \mathsf{F}\{H_y\} \end{bmatrix} e^{jk_x x}\,dk_x. \tag{23}$$

The four matrix elements in brackets, which can be defined as $A'_{11}, A'_{12}, A'_{21}$ and A'_{22} are, respectively, A_{33}, A_{35}, A_{53}, and A_{55} from (18) above. Because this is a 1-D field, $k_o = k_x$. For the initial plane wave field $E_z = \eta H_y = E_o\cos(\omega t_o - kx)$, the operations in (23) can be carried out analytically, first yielding the spectral-domain expressions $\mathsf{F}\{E_z\} = \eta\mathsf{F}\{H_y\} = \pi\lfloor\delta(k_x+k)e^{j\omega t_o} + \delta(k_x-k)e^{-j\omega t_o}\rfloor$, which are then multiplied by $\bar{\mathbf{A}}'$ and inverse transformed giving the final time stepped fields $E_z = \eta H_y = E_o\cos[\omega(t_o - \tau) - kx]$. Notice that this is an exact result for any τ because (22) contains no approximations in a homogeneous region. Notice also that the distance traveled by the plane wave during one time step can be found from the argument of $\cos[\omega(t_o - \tau) - kx]$ as follows:

$$\omega t_o - \omega\tau - kx = \omega t_o - k(x + \tau v). \tag{24}$$

The distance traveled is, therefore, $\Delta d = \tau v$. For numerical calculations, if the time increment τ is chosen to be $\tau = \Delta x/2v$, then $\Delta d = \Delta x/2$. Therefore the numerical distance traveled in one time step τ is $\Delta x/2$.

B. Numerical Method

The most straightforward way to evaluate (22) numerically is to replace the Fourier transforms with discrete Fourier transforms (DFT's). One time step in 1-D becomes

$$\mathbf{F}(m\Delta k_x) = \sum_{n=0}^{N-1} \mathbf{F}(n\Delta x)e^{-j2\pi mn/N} \tag{25a}$$

$$\mathbf{F}(n\Delta x) = \sum_{m=0}^{N-1} \bar{\mathbf{A}}(n\Delta x, m\Delta k_x)\mathbf{F}(m\Delta k_x)e^{j2\pi mn/N} \tag{25b}$$

where $\mathbf{F}(n\Delta x)$ is the spatial domain field computed at the spatial position $n\Delta x$ and $\mathbf{F}(m\Delta k_x)$ is the spectral domain field at the radian frequency

$$m\Delta k_x = m2\pi/(N\Delta x). \tag{26}$$

Scattering objects in the numerical space are accounted for in the transition matrix $\bar{\mathbf{A}}$ by specifying $v = \sqrt{\mu(x)\varepsilon(x)}$. By requiring that the time step τ remain a fixed constant, the matrix $\bar{\mathbf{A}}$ need only be computed during the initial time step, stored in memory, and recalled at each successive time step when (25b) is calculated. Although the DFT algorithm above is simple, an order of N^2 calculations is required to move the field one time step. A much more efficient numerical algorithm can be developed by replacing the DFT with an FFT. Doing so reduces the number of calculations from the order of N^2 to $N\log N$.

C. Numerical Dispersion

At the nth time step the two-dimensional (2-D) TM mode fields in the numerical grid are assumed to be the following monochromatic plane waves

$$\begin{aligned} E_z^n(i,l) &= E_{zo}e^{-j[2\pi(\tilde{k}_x i\Delta x+\tilde{k}_y l\Delta y)-\omega n\tau]} \\ H_x^n(i,l) &= H_{xo}e^{-j[2\pi(\tilde{k}_x i\Delta x+\tilde{k}_y l\Delta y)-\omega n\tau]} \\ H_y^n(i,l) &= H_{yo}e^{-j[2\pi(\tilde{k}_x i\Delta x+\tilde{k}_y l\Delta y)-\omega n\tau]} \end{aligned} \tag{27}$$

where ω is the wave radian frequency and $\tilde{k}_x, \tilde{k}_y$ are the numerical spectral wave numbers. The plane wave expressions in (27) are substituted into (22), with the Fourier transforms replaced by 2-D forward and inverse DFT's. After one time, step the result is

$$\begin{aligned} &\mathbf{F}e^{-j[2\pi\tilde{k}_x p\Delta x+2\pi\tilde{k}_y q\Delta y-\omega(n+1)\tau]} \\ &\quad= \frac{1}{MN}\sum_{r=0}^{M-1}\sum_{s=0}^{N-1}\bar{\mathbf{A}}e^{j2\pi rp/M}e^{j2\pi sq/N} \\ &\qquad\times\sum_{i=0}^{M-1}\sum_{l=0}^{N-1}\mathbf{F}e^{-j2\pi i(r+\tilde{k}_x/\Delta k_x)}e^{-j2\pi l(s+\tilde{k}_y/\Delta k_y)}e^{j\omega\tau} \\ &\quad= \frac{1}{MN}\sum_{r=0}^{M-1}\sum_{s=0}^{N-1}\left[\frac{1-e^{-j2\pi(r+\tilde{k}_x/\Delta k_x)}}{1-e^{-j2\pi(r+\tilde{k}_x/\Delta k_x)/M}}\right. \\ &\qquad\left.\times\frac{1-e^{-j2\pi(s+\tilde{k}_y/\Delta k_y)}}{1-e^{-j2\pi(s+\tilde{k}_y/\Delta k_y)/N}}\right] \\ &\qquad\times\bar{\mathbf{A}}\mathbf{F}e^{j2\pi rp/M}e^{j2\pi sq/N}e^{j\omega n\tau} \end{aligned} \tag{28}$$

where $\mathbf{F} = [E_{zo}\ H_{xo}\ H_{yo}]^T$ and the transition matrix, which is composed of $A_{33}, A_{34}, A_{35}, A_{43}, A_{44}, A_{45}, A_{53}, A_{54}$, and A_{55} from (18) is (29), shown at the bottom of the page. In (29) $k_o = \sqrt{(r\Delta k_x)^2+(s\Delta k_y)^2}$ and $u = k_o v\tau$.

The ratios $\tilde{k}_x/\Delta k_x$ and $\tilde{k}_y/\Delta k_y$ are integers because DFT's only operate at discrete frequencies, which are specified in (26). Therefore in (28) the two summations, together with the two terms in the brackets are zero except when

$$r = -\tilde{k}_x/\Delta k_x, \quad s = -\tilde{k}_y/\Delta k_y \tag{30}$$

at which point they are respectively equal to the integers M and N. Equation (28) then reduces to

$$(\bar{\mathbf{A}}' - \bar{\mathbf{I}}e^{j\omega\tau})\mathbf{F} = 0 \tag{31}$$

where the matrix $\bar{\mathbf{A}}$ with the replacements given in (30) becomes $\bar{\mathbf{A}}'$. Equation (31) is an eigenvalue equation whose determinant, when set to zero, gives

$$\tilde{k}_x'^2 + \tilde{k}_y'^2 = \left(\frac{\omega}{v}\right)^2 = k^2 \tag{32}$$

with $\tilde{k}_x' = 2\pi\tilde{k}_x$ and $\tilde{k}_y' = 2\pi\tilde{k}_y$. The numerical wave numbers can be expressed in terms of ϕ, the angle at which the wave propagates with respect to the x-axis, and the numerical space propagation constant $\tilde{k}'$ by $\tilde{k}_x' = \tilde{k}'\cos\phi$, $\tilde{k}_y' = \tilde{k}'\sin\phi$. These two relations when substituted into (32) give

$$\tilde{k}' = k. \tag{33}$$

The conclusion we reach from this exercise is that the path integral time-domain method does not suffer from numerical dispersion regardless of the direction in which waves travel in the numerical lattice.

D. Stability

Fourier transformation is a unitary operation, and therefore is unconditionally stable. Since the product of unitary operators is also unitary, the operator here $(\mathsf{F}\bar{\mathbf{A}}\mathsf{F}^{-1})$, which consist of forward and inverse Fourier transforms and multiplication by the transition matrix, is unitary if it can also be shown that the matrix $\bar{\mathbf{A}}$ is unitary. A quick calculation $\overline{\mathbf{A}}\ \overline{\mathbf{A}}^{-1} = \bar{\mathbf{I}}$ shows that this is indeed the case. However, under certain conditions we have observed what appears to be instability. In the following paragraph, we offer an explanation and method for overcoming this difficulty.

In the theory of state variables, it is well known [20] that the eigenvalues of $\bar{\mathbf{S}}(\mathbf{r},\mathbf{k})$ in the operator $e^{\bar{\mathbf{S}}(\mathbf{r},\mathbf{k})\tau}$, which becomes the transition matrix $\bar{\mathbf{A}}$ are the poles of the transfer function. It can be shown that, for the electromagnetic field in a lossless region, these poles lie in symmetric pairs on the complex axis. For this reason the analytic operator $\bar{\mathbf{A}}$ can be described as

$$\bar{\mathbf{A}} = \begin{bmatrix} \cos u & \frac{-j\eta s\Delta k_y}{k_o}\sin u & \frac{j\eta r\Delta k_x}{k_o}\sin u \\ \frac{-js\Delta k_y}{\eta k_o}\sin u & \frac{(r\Delta k_x)^2+(s\Delta k_y)^2\cos u}{k_o^2} & \frac{(r\Delta k_x)(s\Delta k_y)(1-\cos u)}{k_o^2} \\ \frac{jr\Delta k_x}{\eta k_o}\sin u & \frac{(r\Delta k_x)(s\Delta k_y)(1-\cos u)}{k_o^2} & \frac{(s\Delta k_y)^2+(r\Delta k_x)^2\cos u}{k_o^2} \end{bmatrix} \tag{29}$$

being marginally stable. However, through numerical roundoff error, the poles of the transfer function (i.e., the operator $\bar{\mathbf{A}}$) can "drift" into the right half plane causing instability. This situation can be remedied by adding a small loss (σ) everywhere in the numerical scattering region. The eigenvalues of $\bar{\mathbf{S}}(\mathbf{r},\mathbf{k})$ will then contain a small negative real part. The poles of the transfer function are thereby moved a short distance into the left half of the complex plane, thus preventing numerical instability in the computed fields.

An example can be easily constructed for a 1-D case in which a plane wave propagates in a lossy inhomogeneous region, by repeating the operations that lead to (21) with the stipulation $(\sigma \neq 0, \rho^* = 0)$. The elements in the bracketed matrix in (23) become

$$\begin{aligned} A'_{11} &= \frac{\lambda_2 e^{\lambda_1 \tau} - \lambda_1 e^{\lambda_2 \tau}}{-2j\beta} \\ A'_{12} &= \frac{k_x}{2\varepsilon}\left[\frac{e^{\lambda_1 \tau} - e^{\lambda_2 \tau}}{\beta}\right] \\ A'_{21} &= \frac{k_x}{2\eta}\left[\frac{e^{\lambda_1 \tau} - e^{\lambda_2 \tau}}{\beta}\right] \\ A'_{22} &= \frac{\lambda_1 e^{\lambda_1 \tau} - \lambda_2 e^{\lambda_2 \tau}}{-2j\beta} \end{aligned} \tag{34}$$

where

$$\lambda_{\frac{1}{2}} = \alpha \pm j\beta \tag{35}$$

$$\alpha = \frac{\sigma}{2\varepsilon}, \quad \beta = \begin{cases} \sqrt{(k_x v)^2 - \left(\frac{\sigma}{2\varepsilon}\right)^2}, & |k_x v| \geq \frac{\sigma}{2\varepsilon} \\ -j\sqrt{\left(\frac{\sigma}{2\varepsilon}\right)^2 - (k_x v)^2}, & |k_x v| \leq \frac{\sigma}{2\varepsilon} \end{cases}. \tag{36}$$

The matrix elements in (34) can be shown to reduce to those in (23) in the limit $\sigma \to 0$.

E. Accuracy

In an inhomogeneous space, (22) gives an exact solution for the time evolution of the field. However, because the Fourier transform usually cannot be evaluated analytically in practical scattering situations, it is replaced by a DFT. The difference between the discrete and continuous transforms is attributed to the discrete transform requirements for sampling and truncation. The validity of this approximation is strictly a function of the wavefunction being analyzed [21]. For these two transforms to be equivalent the distribution function must be periodic, it must be bandwidth limited, and each dimension of the numerical space must span one or multiple periods of the distribution function. Also the Nyquist limit, a requirement that the sampling interval must be at least two times the highest frequency component of the distribution function, must be met. If all of these conditions are not met the two primary sources of error are termed leakage and aliasing. Applying a numerical filter to the spatial or frequency-domain distribution function can reduce both of these types of errors.

In the PITD method the distribution function in the forward Fourier transform is the time-domain electromagnetic field and in the inverse transform it is the product of the spatial frequency spectrum of the field and the transition matrix $\bar{\mathbf{A}}$, which accounts for all physical objects in the scattering space. The scattering space is, in general, not periodic and because the dielectric constant changes discontinuously between air and any material bodies in the numerical region, it is usually not bandwidth limited.

Our initial attempts to reduce errors by implementing standard numerical filters, such as a Parzen, Hanning, or Welch window, did not give satisfactory results. The cumulative effect is that of raising any filter to a power equal to the number of time steps. However, the absorbing boundary condition described in the next section, acts both as a satisfactory numerical filter and wave-absorbing method.

It should be noted that the discussion above concerns numerical error in an inhomogeneous region. However, with numerical techniques it is customary to first consider the inherent error caused by making numerical approximations to derivatives or integrals in the mathematical expression of the method in a homogeneous region. For example the most common finite difference approximation of a first-order derivative is said to have an accuracy on the order of $(\Delta x)^2$. With the PITD method it is significant that the usual time-domain excitation functions, a single-frequency sinusoid or any bandwidth limited function such as a truncated Gaussian pulse can virtually propagate indefinitely in the numerical space without error. This is possible because these excitations meet the conditions that prevent leakage and aliasing errors. However, a key factor is that the FFT propagates the highest frequency component at the Nyquist limit, as will be demonstrated below. Error will, therefore, be accumulated only in the last digits, due to the usual multiplication and division round off errors.

F. Absorbing Boundary Conditions

In a time-domain computational space an absorbing boundary condition (ABC) is required in order to annihilate outward propagating electromagnetic waves at the numerical boundaries. Also an ABC is needed for the PITD method because Fourier transforms, which govern the manner in which propagating and scattered fields are manipulated in the numerical space, are subject to what is known as the "wrap-around" effect. For example, fields that propagate to the right in the numerical region disappear on the right side of the numerical boundary while simultaneously reappearing on the left side. In this section, it will be demonstrated that an ABC can be implemented in the PITD numerical code.

For the PITD method in one dimension, an ABC, which is a set of absorbing layers, has been found to be very effective. With this method a nonphysical absorbing zone, made up of several layers with progressively higher conductivity, lies on the sides of the computational domain. This zone is perfectly absorbing if two conditions are met at all frequencies. First, the reflection coefficient must be zero at the interface between the computational region and absorbing zone and second the wave impedance in the absorbing zone must be a constant. If σ and ρ^* denote the

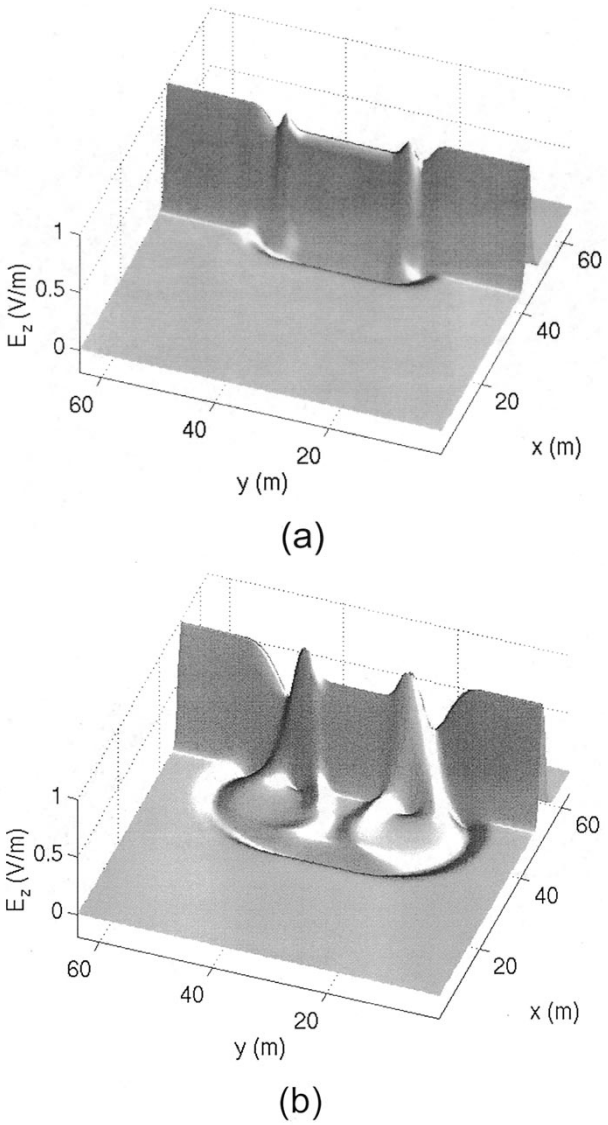

Fig. 1. The total electric field E_z component of a TM polarized plane wave Gaussian pulse in air incident on a 2-D dielectric cylinder with $\varepsilon_r = 1.75$ and $\mu_r = 1.0$.

respective electric conductivity and magnetic resistivity in the absorbing zone, the essential matching condition is given by

$$\frac{\sigma}{\varepsilon_o} = \frac{\rho^*}{\mu_o}. \tag{37}$$

As an example, by repeating the operations that lead to (21) and enforcing (37) and the stipulation that $(\sigma \neq 0, \rho^* \neq 0)$, the 1-D absorbing zone equations are found to be those in (23) with a factor $e^{-\sigma\tau/\varepsilon_o}$ multiplying the otherwise unchanged bracketed matrix term in (23). The number of absorbing layers and the choice of a loss function σ governs absorption. A common choice for conductivity is one that is a parabolic function of depth [22]. For the numerical results given below, σ at the ith layer is

$$\sigma_i = \frac{\sigma_m}{\delta^2}\left((i\Delta x)^2 + \frac{(\Delta x)^2}{12}\right) \tag{38}$$

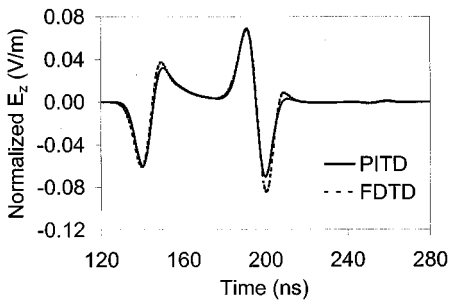

Fig. 2. The time history of the E_z component of the total electric field due to a plane wave Gaussian pulse incident on a rectangular dielectric cylinder with $\varepsilon_r = 1.75$ and $\mu_r = 1.0$.

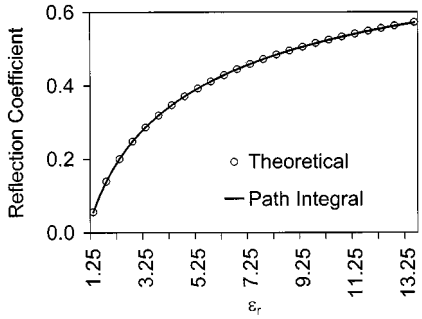

Fig. 3. Reflection coefficient as a function of dielectric constant for the 1-D case of a plane wave incident on a dielectric half space.

with

$$\sigma_m = \frac{3\varepsilon_o c \ln R}{2\delta}. \tag{39}$$

Here δ is the width of the absorbing zone, which in the results below has nine layers and R is chosen to be 10^{-5}.

III. Results

Fig. 1 shows a plane wave Gaussian pulse incident on a dielectric cylinder in 2-D. The incident field is transverse magnetic (TM) to the z-direction (i.e., it contains E_z, H_x, and H_y components) and propagates in the x-direction. The transition matrix for this case is given in (29). Fig. 1(a) is a plot of the total electric field in a 256×256 square grid with $\Delta x = 0.25$ m and $\Delta t = \Delta x/c$ as it initially contacts the rectangular dielectric cylinder which occupies a 40×95 grid area $40\text{ m} \leq x \leq 50$ m, $20\text{ m} \leq y \leq 43.75$ m. Fig. 1(b) shows the field 30 time steps later.

Fig. 2 shows the time history of the E_z component of the total electric field collected at $x = 31.5$ m, $y = 29.0$ m in front of a rectangular dielectric cylinder with $\varepsilon_r = 1.75$ located at $34\text{ m} \leq x \leq 40$ m, $34\text{ m} \leq y \leq 40$ m in a numerical space 63.75-m square computed with the PITD and FDTD methods. The incident field is a TM plane wave traveling in the x-direction and containing a Gaussian profile $\exp(-(n-4\beta)^2/\beta^2)$ where n is the time step and $\beta = 7$ for the path integral, $\beta = 14$ for FDTD. The numerical space grid size is $\Delta x = \Delta y = 0.25$ m and the time step is $\Delta t = \Delta x/c$ and $\Delta t = \Delta x/2c$ for PITD

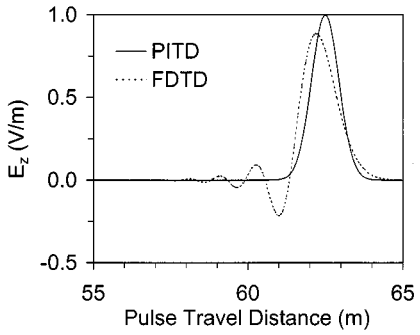

Fig. 4. Illustration of numerical dispersion by comparison of Gaussian pulses that have propagated approximately 500 lattice points in homogeneous FDTD and PITD numerical lattices.

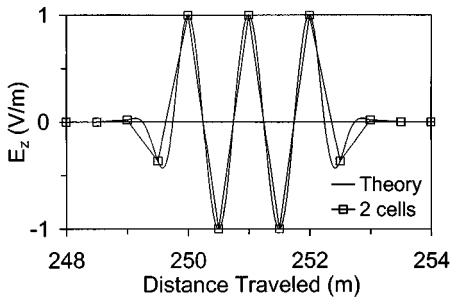

Fig. 5. Illustration that the Nyquist limit is reached by PITD by comparison of an exact (smooth curve) and a PITD single frequency pulse that has propagated through approximately 500 lattice points with two points per wavelength.

and FDTD, respectively. The difference between the results obtained by these two methods can be attributed to dispersion in the high-frequency FDTD components.

Fig. 3 shows a comparison of the exact and PITD computed reflection coefficients for a 1-D plane wave incident from air on a dielectric half-space. Exact and path integral time-domain method results are plotted as a function of the half-space dielectric constant. This indicates that the PITD method remains stable and accurate even when the field is reflecting from and propagating through a region with a high refractive index.

Fig. 4 pictures a comparison of path integral and FDTD method Gaussian pulses that have propagated approximately 500 lattice points in their respective numerical lattices. In each case $\Delta = 0.125$ and $\Delta t = \Delta x/2c$. Initially, each Gaussian pulse is formed according to $\exp\{-[((i/2) - 4\beta)/\beta]^2\}$, where i is the spatial grid point index. The parameter β is chosen to be ten so that with the FDTD method, dispersion is minimized and the highest frequency propagates at the FDTD limit, four points per wavelength. Nonetheless, it is clear from the figure that numerical dispersion degrades FDTD calculated fields that have propagated a significant distance. In this case, the highest frequency component has propagated only 50 wavelengths. As predicted above, the PITD fields are unaffected by numerical dispersion.

Fig. 5 shows a PITD computed single frequency signal that has been "ramped up" over two cycles and propagated a distance of approximately 250λ compared with a plot of the exact excitation. The PITD result is obtained with two cells per wavelength $\Delta x = 0.5$ m, $\beta = 10$, and $\Delta t = \Delta x/2c$. From the figure it is seen that the $(2\text{-cell}/\lambda)$ signal has not dispersed after propagating through 500 lattice points. This result is evidence that the PITD method is not subject to numerical dispersion even at the Nyquist limit.

In Fig. 6 local error for the 1-D case in which the pulse propagates into an absorbing boundary is shown. The local reflection error pictured in Fig. 6(a) is the difference between the magnitudes of E_z found with and without the absorbing boundary, taken at a point close to the boundary upon which the pulse is incident. The transmission error shown in Fig. 6(b) is the magnitude of E_z that has been transmitted through the boundary and absorbing region by the wrap-around effect. Since all calculations are made in single precision with an initial Gaussian pulse amplitude of 1 V/m, it appears that little if any field has reflected

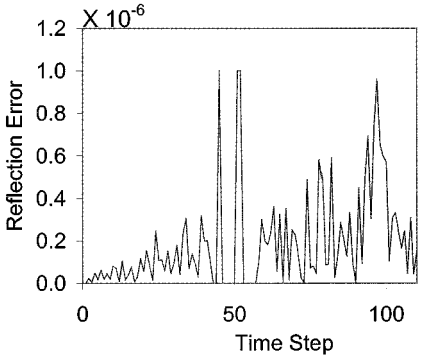

(a)

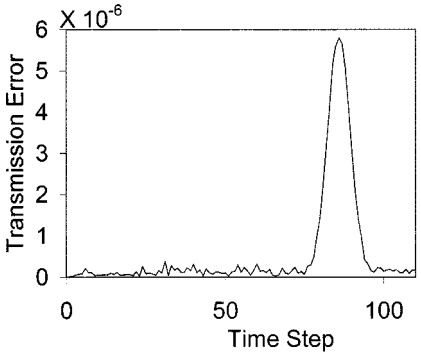

(b)

Fig. 6. Berenger ABC error for the electric field (a) reflected and (b) transmitted through the numerical boundary due to the "wrap around" effect.

from the absorbing boundary. The field that has passed through the absorbing boundary is also close to the machine noise level.

IV. Conclusion

We have presented a promising new method for calculating the complete full wave time-domain scattered electromagnetic field, formulated as a path integral. We have also presented a method by which it can be easily and efficiently evaluated. This numerical procedure, described as the PITD method, contains a simple sequence of operations requiring only a forward and an inverse Fourier transform with an intervening coefficient matrix multiplication. Because fast Fourier transforms carry the primary computational burden, its CPU time is competitive with other methods.

It is shown both analytically and numerically that the PITD method yields a field that is not subject to numerical dispersion even at the Nyquist limit. It has also been shown that the PITD method is at least conditionally stable and unconditionally stable when a small amount of loss is added to the scattering region. An advantage of the PITD method is that its stability does not depend upon the relationship between τ and Δx. Remarkably, the path integral time-domain method has been shown to have no error when the excitation is bandlimited as it is with a Gaussian pulse or a single frequency signal in a homogeneous space.

In 1-D an absorbing boundary condition has been found to be effective at preventing both reflection and the FFT "wrap around" effect at the numerical boundaries. Because this condition forces the fields to zero at the numerical boundary it is also an effective numerical filter, which helps lessen aliasing and leakage errors. The absorbing layer ABC can be implemented in 2-D and 3-D just as described for the 1-D case in the text. The Berenger condition, which is more effective than absorbing layers, can in theory be implemented in the 2-D and 3-D PITD, although we have not yet done so.

We conclude that the path integral time-domain method arises as a possible alternative to other time-domain methods. Of course, much more research will be needed to determine were the pros and cons of this method will place it in the menu of currently available techniques.

APPENDIX

The propagator $\bar{\mathbf{K}}$ is not a Green's function since it satisfies the *homogeneous* equation $(\partial\bar{\mathbf{K}}/\partial t) - \bar{\mathbf{S}}\bar{\mathbf{K}} \doteq \mathbf{L}\bar{\mathbf{K}} = 0$ (10), subject to the initial condition in (11). The differential equation $\mathbf{LF} = 0$ (7) is satisfied because operating on (19) with $\mathbf{L}$ gives

$$\begin{aligned}\mathbf{LF} &= \mathbf{L}\int_{-\infty}^{\infty} \bar{\mathbf{K}}(\mathbf{r},\mathbf{r}';\tau)\mathbf{F}_o(\mathbf{r}',t')\,d\mathbf{r}' \\ &= \int_{-\infty}^{\infty} \{\mathbf{L}\bar{\mathbf{K}}(\mathbf{r},\mathbf{r}';\tau)\}\mathbf{F}_o(\mathbf{r}',t')\,d\mathbf{r}' = 0. \quad \text{(A.1)}\end{aligned}$$

The initial condition is satisfied because in the limit as $t \to t'$, (19) becomes

$$\begin{aligned}\mathbf{F}(\mathbf{r},t') &= \int_{-\infty}^{\infty} \bar{\mathbf{K}}(\mathbf{r},t';\mathbf{r}',t')\mathbf{F}_o(\mathbf{r}',t')\,d\mathbf{r}' \\ &= \int_{-\infty}^{\infty} \delta(\mathbf{r}-\mathbf{r}')\mathbf{F}_o(\mathbf{r}',t')\,d\mathbf{r}' = \mathbf{F}_o(\mathbf{r},t'). \quad \text{(A.2)}\end{aligned}$$

REFERENCES

[1] R. P. Feynman and A. R. Hibbs, *Quantum Mechanics and Path Integrals*. New York: McGraw-Hill, 1965.

[2] C. Huang and R. D. Nevels, "A closed-form multi-dimensional free space Green's function by the path integral method," *Microwave Opt. Technol. Lett.*, vol. 5, no. 5, pp. 225–227, May 1992.

[3] R. D. Nevels, Z. Wu, and C. Huang, "Feynman path integral for an infinite potential barrier," *Phys. Rev. A*, vol. 48, no. 5, pp. 3445–3451, Nov. 1993.

[4] J. B. Keller, "Geometrical theory of diffraction," *J. Opt. Soc. Amer.*, vol. 52, no. 2, pp. 116–130, Feb. 1962.

[5] J. B. Keller and D. W. McLaughlin, "The Feyman integral," *The Amer. Math. Monthly*, vol. 82, no. 5, pp. 451–456, 1975.

[6] V. S. Bushlaev, "Continuum integrals and the asymptotic behavior of the solutions of parabolic equations as $t \to 0$. Applications to diffraction," in *Topics in Mathematical Physics*, M. Sh. Birman, Ed. New York: Consultants Bureau, 1968, vol. 2.

[7] V. I. Klyatskin and V. I. Tatarskii, "The parabolic equation approximation for propagation of waves in a random medium with random inhomogeneities," *Sov. Phys. JETP*, vol. 31, no. 2, pp. 335–339, 1970.

[8] P. L. Chow, "A function phase-integral method and applications to the laser beam propagation in random media," *J. Stat. Phys.*, vol. 12, no. 2, pp. 93–109, 1975.

[9] R. Dashen, "Path integrals for waves in random media," *J. Math. Phys.*, vol. 20, no. 5, pp. 894–920, 1979.

[10] V. U. Zavorotny, "Strong fluctuations of electromagnetic waves in a random medium with finite longitudinal correlation of the inhomogeneities," *Sov. Phys. JETP*, vol. 48, no. 1, pp. 27–31, 1978.

[11] I. M. Besieris, "Wave-kinetic method, phase-space path integrals, and stochastic wave propagation," *J. Opt. Soc. Amer. A*, vol. 2, no. 12, pp. 2092–2099, Dec. 1985.

[12] J. Gozani, "Two-scale expansion of wave propagation in a random medium," *Comp. Phys. Comm.*, vol. 65, no. 1–3, pp. 117–120, 1991.

[13] M. Eve, "The use of path integrals in guided wave theory," *Proc. Roy. Soc. London*, pt. A, vol. 347, pp. 405–417, 1976.

[14] C. C. Constantinou and R. C. Jones, "Path-integral analysis of tapered, graded-index waveguides," *J. Opt. Soc. Amer. A*, vol. 8, no. 8, pp. 1240–1244, Aug. 1991.

[15] R. H. Hardin and F. D. Tappet, "Applications of the split-step Fourier method to the numerical solution of nonlinear and variable coefficient wave equations," *SIAM Rev.*, vol. 15, p. 423, 1973.

[16] H. V. Hitney, "A practical tropospheric scatter model using the parabolic equation," *IEEE Trans. Antennas Propagat.*, vol. 41, pp. 905–909, July 1993.

[17] G. D. Dockery and J. R. Kuttler, "An improved impedance-boundary algorithm for Fourier split-step solutions of the parabolic wave equation," *IEEE Trans. Antennas Propagat.*, vol. 44, pp. 1592–1599, Dec. 1996.

[18] R. D. Nevels, C. Huang, and Z. Wu, "The Fourier transform path integral method—A numerical technique for scalar scattering in inhomogeneous regions," *Proc. Inst. Elect. Eng.*, pt. H, pp. 488–492, Nov. 1993.

[19] G. Barton, *Elements of Green's Functions and Propagation*. Oxford, U.K.: Oxford Sci. Clarendon, 1989.

[20] P. M. DeRusso, R. J. Roy, C. M. Close, and A. A. Desrochers, *State Variables for Engineers*. New York: Wiley, 1998.

[21] E. O. Brigham, *The Fast Fourier Transform*. Englewood Cliffs, NJ: Prentice-Hall, 1974.

[22] J.-P. Berenger, "A perfectly matched layer for the absorption of electromagnetic waves," *J. Computat. Phys.*, vol. 114, pp. 185–200, 1994.

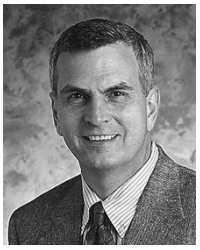

Robert D. Nevels (S'72–M'77–SM'86) received the B.S.E.E. degree from the University of Kentucky, Lexington, the M.S.E.E. degree from Georgia Tech, Atlanta, and the Ph.D. from the University of Mississippi, University, in 1969, 1973, and 1979, respectively.

In 1978, he joined Texas A&M University as an Assistant Professor. He became a Full Professor in 1993 and is currently Assistant Department Head. During the summer of 1992 he was a Visiting Professor at the Institute for Light Sources, Fudan University, Shanghai, China. He was associate editor of the four-volume book series *Handbook of Microwave and Optical Components* (New York: Wiley, 1990–1992). He is currently Associate Editor of the *Microwave and Optical Technology Letters*. His interests are in analytical and numerical techniques for electromagnetic scattering, antennas, and microwave device design.

Dr. Nevels is currently a member of the IEEE Antennas and Propagation Society ADCOM, Chairman of the IEEE-AP Man and Radiation Committee, and General Chairman of the 2002 IEEE Antennas and Propagation International Conference. He served as Associate Editor of the IEEE TRANSACTIONS ON ANTENNAS AND PROPAGATION from 1986 to 1989. He has received eight teaching awards, including the IEEE Outstanding Educator Award of Region 5 for 1997. He is a member of Eta Kappa Nu, Sigma Xi, Commission B of URSI, the Electromagnetics Academy, and the American Scientific Affiliation.

Jeffrey A. Miller was born in San Diego, CA, in 1965. He received the B.S. and M.S. degrees in electrical engineering from Texas A&M University, College Station, in 1987 and 1989, respectively. He is currently working toward the Ph.D. degree in electrical engineering from the same university.

From 1989 to 1991, he was employed by Texas Instruments, McKinney, TX, to design and analyze broad-band antennas. From 1991 to 1996 he worked at Northrop Grumman, Pico Rivera, CA, in low observable technology. Since 1997, he has been at Texas A&M University primarily as a Graduate Research Assistant investigating the path-integral time-domain method. His current research interests include computational electromagnetics; massively parallel computer systems as well as emerging computer architectures and their application to electromagnetics. He is also interested in engineering education.

Richard E. Miller received the B.S., M.S., and Ph.D. degrees in electrical engineering from Texas A&M University, College Station, in 1987, 1989, and 1999, respectively.

From 1989 to 1991, he was an Antenna Engineer at Texas Instruments, Inc. (now Raytheon TI Systems), McKinney, TX. From 1991 to 1996 he was a Radar Cross Section Engineer at Northrop (now Northrop Grumman), Pico Rivera, CA. Since 1999 he has worked on phased-array radar antennas at Lockheed Martin Government Electronic Systems, Moorestown, NJ.

Dr. Miller is a member of the IEEE Antenna and Propagation, Signal Processing, and Education Societies.